

Semiclassical approach to finite temperature quantum annealing with trapped ions

David Raventós,^{1,*} Tobias Graß,² Bruno Juliá-Díaz,^{3,4,1} and Maciej Lewenstein^{1,5}

¹*ICFO-Institut de Ciències Fotoniques, The Barcelona Institute of Science and Technology, 08860 Castelldefels (Barcelona), Spain*

²*Joint Quantum Institute, University of Maryland, College Park, MD 20742, U.S.A.*

³*Departament de Física Quàntica i Astrofísica, Facultat de Física, Universitat de Barcelona, Barcelona 08028, Spain*

⁴*Institut de Ciències del Cosmos, Universitat de Barcelona, ICCUB, Martí i Franquès 1, Barcelona 08028, Spain*

⁵*ICREA, Passeig de Lluís Companys, 23, 08010 Barcelona, Spain*

Abstract

Recently it has been demonstrated that an ensemble of trapped ions may serve as a quantum annealer for the number-partitioning problem [Nature Comm. DOI: 10.1038/ncomms11524]. This hard computational problem may be addressed employing a tunable spin glass architecture. Following the proposal of the trapped ions annealer, we study here its robustness against thermal effects, that is, we investigate the role played by thermal phonons. For the efficient description of the system, we use a semiclassical approach, and benchmark it against the exact quantum evolution. The aim is to understand better and characterize how the quantum device approaches a solution of, an otherwise, difficult to solve NP-hard problem.

I. INTRODUCTION

Quantum computers and quantum simulators are nowadays becoming a reality thanks to the advances in ion trapping and integrated superconducting technology [1–5]. A possible device which is quickly being developed are quantum annealers. Annealing, as opposed to quenching, is a method to produce the ground state of a target Hamiltonian by slowly deforming/adjusting a well-known ground state of a different Hamiltonian. Annealing is in fact a concept originating from classical metallurgy, extended in the 1980s to classical optimization problems, and known as simulated annealing [6, 7]. In the current quantum versions, quantum annealing is very much analogous to quantum adiabatic computing, but is typically targeted towards the classical optimization problems. The idea is to add a simple, noninteracting, but noncommuting term to the original classical Hamiltonian. This simple additional term should dominate the system at the initial time, so that the ground state will be easy to find, since it will correspond to a non-interacting system. The non-commuting nature of the additional term ensures that the initial and target ground states are not symmetry protected. Then, the additional term is adiabatically removed and the ground state is expected to go slowly from the initial one to the one of the Hamiltonian of interest [8–10], see also the recent review [11]. This scheme is nowadays plausible with a large number of possible platforms, including trapped ions, cavity QED, circuit QED, superconducting junctions [12] and atoms in nanostructures. The first commercially accessible quantum annealers are in the market [13–15].

Since the original proposals [16, 17] trapped ions quantum simulators are the subject of intensive theoretical

and experimental research. Starting from realization of the simple instances of quantum magnetism [18], they have reached quite a maturity in the recent experimental developments (cf. [19–25]). The recent paper by Bollinger’s group [26], in addition to the excellent experimental work, contains also an outstanding analysis of quantum dynamics of the relevant Dicke model, in which the ions interact essentially with one phononic mode.

Quantum dynamics in general, and in particular for the Dicke-like ion-phonon models, are very challenging for numerical simulations. Exact treatments are possible for small systems only, so that various approximate methods have to be used. One of them is the truncated Wigner approximation, in which both ionic and phononic operators are replaced by complex numbers, the dynamics becomes “classical”, and only the initial data mimic the “quantumness” of the problem [27]. This approach was used in Ref. [28] to study the quantum non-equilibrium dynamics of spin-boson models. More sophisticated “mean-field” approaches decorrelate ions from phonons, but treat at least either ions or phonons fully quantum mechanically – this approach is in particular analyzed in the present paper. Quantum aspects of the models in question were studied in the series of papers [29–31].

We have considered recently the exact quantum dynamics of few ion systems to demonstrate the robustness of chiral spin currents in a trapped-ion quantum simulator using Floquet engineering [32]. Our earlier works include studies of dual trapped-ion quantum simulators as an alternative route towards exotic quantum magnets [33], and studies of ion chains with long range interactions forming “magnetic loops” [34]. Topological edge states in periodically-driven trapped-ion chains [35], trapped ion quantum simulators of Rabi lattice models with discrete gauge symmetry [36], and hidden frustrated interactions and quantum annealing in trapped ion spin-phonon chains [37] were also considered recently. Novel ideas for spin-boson models simulated with trapped ions

* David.Raventos@icfo.eu

can be found in Ref. [38].

In Ref. [39], it has been proposed to use trapped ions for solving difficult optimization problems via quantum annealing. Such scheme, applied to the concrete example of number-partitioning, has come under scrutiny in Ref. [40]. The idea is to profit from the known mapping between the number partitioning problem and the ground state of spin Hamiltonians [41]. In the interesting domain, where the number partitioning problem is notably difficult, the system is actually in the spin-glass-like phase, which renders finding the actual ground state an involved task for classical methods. The annealing method proposed was found to work well for small number of ions at zero temperature. In this work we explore in detail a semiclassical approximation to the original problem, where the quantum correlations between the spins and the phonon bath are neglected. This, however, allows us to solve the Heisenberg equations of motion in an efficient way for much larger ion systems. Notably, the approach allows us to explore finite temperature effects on the annealing protocol.

Our present work is structured as follows. In Sec. II we explain the specific technical details of the studied model and the calculations. In particular, the Hamiltonian is explained in II A, the reduction methods in II B and the annealing protocol II C along with the basic definitions II D. In Sec. III, we introduce our semiclassical approximation, and benchmark it with a full quantum treatment. In Sec. IV we show the results of the semiclassical approach applied to finite temperature. Here, we set the initial phonon population to non-zero thermal values. A summary and our main conclusions are provided in Sect. V. Finally, in the appendix we provide some further tests to our numerical integration method (appendix A), and a brief study of the optimal bias for the annealing protocol (appendix B).

II. SYSTEM

A. Hamiltonian

We study a chain of N trapped ions interacting by effective spin-spin interactions subjected to a transverse time-dependent magnetic field. Interactions are generated by Raman coupling the pseudo-spin degrees of freedom to the phonon modes which are obtained expanding the Coulomb force between the ions around their equilibrium positions [17]. The phonon spectrum is defined through its natural frequencies ω_k and modes ξ_k^i . The dynamics of the system is described by a time-dependent Hamiltonian that in the Schrödinger picture reads,

$$\begin{aligned} \mathcal{H}_S(t)/\hbar = & \sum_k^M \omega_k \hat{a}_k^\dagger \hat{a}_k + \sum_{i,k}^{N,M} \Omega \eta_k^{(i)} \sin(\omega_L t) \left(\hat{a}_k^\dagger + \hat{a}_k \right) \sigma_x^{(i)} \\ & + \sum_i^N B(t) \sigma_z^{(i)} + \varepsilon \sigma_x^{(p)}, \end{aligned} \quad (1)$$

where \hat{a}_k (\hat{a}_k^\dagger) is the annihilation (creation) operator of one phonon in the k -th mode and ω_k is the frequency of that mode. The operators $\sigma_x^{(i)}$, $\sigma_y^{(i)}$, and $\sigma_z^{(i)}$ are the spin operators in the i -th position. The frequencies Ω and ω_L are the Rabi frequency and the beatnote frequency of the laser, respectively. The dimensionless parameters $\eta_k^{(i)}$ are the Lamb-Dicke parameters proportional to the displacement of an ion i in the vibrational mode k , see Ref. [17]. As usual, t is time, and a time-dependent magnetic field $B(t)$ allows us to perform the quantum annealing. A small bias term, proportional to ε , has been added in the p -th position to remove the \mathcal{Z}_2 degeneracy. The upper limit of the sum over the ions i is N , the number of ions. The upper limit of the sum in modes k is M , the number of modes. The total number of phonon modes is $3N$, but the Raman beam couples to only N modes, selected by the wave vector difference of the lasers. At this point, we may keep our analysis general by making no assumption about the number M of modes. However, all phonons which are considered are assumed to be coupled to the spin in the same way. Hereinafter, the upper limits of the sums will be omitted for brevity.

B. Equations of motion

We compute the Heisenberg equations of motion for the quantum average of every operator in the Hamiltonian, \hat{a}_k , \hat{a}_k^\dagger , $\sigma_x^{(i)}$, $\sigma_y^{(i)}$, and $\sigma_z^{(i)}$. Given that these are time independent operators, the calculation reduces to commutators. Additionally, we replace $\hat{a}_k^\dagger + \hat{a}_k$ by $2\Re[\hat{a}_k]$ and $\hat{a}_k - \hat{a}_k^\dagger$ by $2i\Im[\hat{a}_k]$. The equations of motion (all with real coefficients) read,

$$\begin{aligned} \frac{d\langle \Re[\hat{a}_k] \rangle}{dt} &= \omega_k \langle \Im[\hat{a}_k] \rangle \\ \frac{d\langle \Im[\hat{a}_k] \rangle}{dt} &= -\omega_k \langle \Re[\hat{a}_k] \rangle - \sin(\omega_L t) \sum_j \Omega \eta_k^{(j)} \langle \sigma_x^{(j)} \rangle, \\ \frac{d\langle \sigma_x^{(i)} \rangle}{dt} &= -2B(t) \langle \sigma_y^{(i)} \rangle, \\ \frac{d\langle \sigma_y^{(i)} \rangle}{dt} &= -4 \sum_l \Omega \eta_l^{(i)} \sin(\omega_L t) \langle \Re[\hat{a}_l] \sigma_z^{(i)} \rangle \\ &\quad + 2B(t) \langle \sigma_x^{(i)} \rangle - 2\varepsilon \langle \sigma_z^{(i)} \rangle \delta_{p,i}, \\ \frac{d\langle \sigma_z^{(i)} \rangle}{dt} &= 4 \sum_l \Omega \eta_l^{(i)} \sin(\omega_L t) \langle \Re[\hat{a}_l] \sigma_y^{(i)} \rangle + 2\varepsilon \langle \sigma_y^{(i)} \rangle \delta_{p,i}. \end{aligned} \quad (2)$$

C. Annealing protocol

The functional form and value of Ω , $B(t)$ and ε determine the annealing protocol. In these annealing schemes, the initial value of the transverse magnetic field $B(t=0)$ must be sufficiently strong to initialize the system in the paramagnetic phase, that is, B must be larger than

the effective spin-spin interactions $J \sim \Omega^2 \omega_{\text{rec}} / (\delta \omega_{\text{rad}})$, where ω_{rec} is the recoil energy of the photon-ion coupling, ω_{rad} is the radial trap frequency, and δ the detuning from the nearest phonon mode. For typical values, e.g. $\Omega \sim \delta \sim 100$ kHz, $\omega_{\text{rec}} \sim 25$ kHz, $\omega_{\text{rad}} \sim 5$ MHz, we obtain effective interactions $J \sim 1$ kHz, so we need an initial field strength $B(0) \sim 10$ kHz. The annealing scheme proceeds by turning down the magnetic field according to some functional form in order to adiabatically achieve the ground state of the Hamiltonian of interest. Given the adiabatic theorem, for a closed system initialized in the ground state, the final system is guaranteed to be in the ground state as long as the system is gapped along the annealing path, and the variation is slow enough. Generalization to open systems has been proposed in Ref. [42].

We have used a decreasing exponential form for the transverse magnetic field, $B(t) = B(0) e^{-t/\tau}$ with a decay rate τ . The other parameters, Ω and ε , remain constant. An example of the evolution of the system under this protocol is shown in Fig. 1. Initially, $\langle \hat{\sigma}_x^{(i)} \rangle = 0$ for all i , and the total phononic population is set to 0. Within tens of microseconds the phononic modes are populated. Not surprisingly, the mode next to the resonance becomes the most populated one, with a population being orders of magnitude larger than the population of the other modes. In contrast to these rapid changes of the phonon state, the spin dynamics is much slower. The spin expectations $\langle \hat{\sigma}_x^{(i)} \rangle$ remain mostly clustered around zero for hundreds of microseconds. When $B(t) \simeq \varepsilon$, the values $\langle \hat{\sigma}_x^{(i)} \rangle$ start to deviate from zero, and some acquire positive values, while others become negative. Thus, the spin curves separate from each other, and we call the time at which this happens the *separation time*. At some point after the separation time, the spin curves saturate, that is, from then on $\langle \hat{\sigma}_x^{(i)} \rangle$ remain constant in time. We define the *waiting time* as the time when all $\langle \hat{\sigma}_x^{(i)} \rangle$ have stopped varying. At the waiting time, the phononic populations stabilize around certain values, although their oscillations do never vanish.

The quantum annealer produces final values of $\langle \hat{\sigma}_x^{(i)} \rangle$ which are not fully polarized, that is, $|\langle \hat{\sigma}_x^{(i)} \rangle| < 1$. Thus, the final state differs from the classical ground state of the target Hamiltonian, that is, the Hamiltonian in the absence of a transverse field. Thus, we take as readout of the annealing protocol the average spin values [43–45]. This is not a problem, as long as for all spins the sign matches with the one in the classical state. As explained in detail in Ref. [40], the spin configuration of the target Hamiltonian is determined by the dominant mode, defined as the one with frequency just below the beatnote frequency ω_L . There are different reasons why the final ground state might show a different spin pattern: Either, the annealing was too fast, that is, the value of τ was chosen too small, or the effective spin model is not valid. This is the case when ω_L is too close to a resonance ω_k .

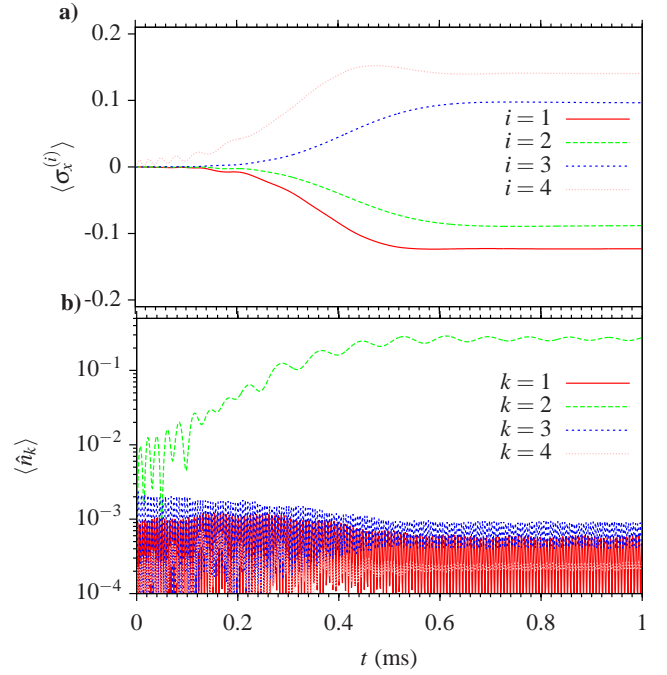


FIG. 1. (Upper panel) Evolution of $\langle \hat{\sigma}_x^{(i)} \rangle$ in a system with 4 spins, with initial populations of phononic modes set to 0. The biased spin is the pink one, see text for details. (Lower panel) Evolution of the populations of the phononic modes in a system with 4 spins, with initial populations of phononic modes set to 0. $\delta = 1$ MHz.

D. Fidelity of the annealing protocol

In order to quantify the success of the annealing protocol, that is, the ability of the method to identify the target ground state of the spin system, we will define the following fidelity,

$$F = \begin{cases} \min_i |\langle \sigma_x^{(i)} \rangle| & \text{if } \text{sign}[\langle \sigma_x^{(i)} \rangle] = \text{sign}[\eta_{k_d}^{(i)}], \forall i \\ 0 & \text{Otherwise} \end{cases}, \quad (3)$$

where η_{ij} is the i th component of the dominant mode k_d for a fixed value of the beatnote frequency ω_L . That is, the fidelity is zero if the signs of $\langle \sigma_x^{(i)} \rangle$ do not match the signs of η_i of the dominant mode. If the signs are reproduced, the value of the fidelity is defined as the smallest expectation value of the spins of the ions. Note that with this definition, any non-zero fidelity is good enough for correctly identifying the ground state pattern, assuming the absence of noise in the system.

III. SEMICLASSICAL APPROXIMATION

A. Semiclassical equations of motion

Now we will develop a semiclassical approximation to the exact equations of motion, Eq. (2), that will allow us

to study larger systems of ions and the effects of temperature on the annealing protocols. We make the following approximations:

$$\begin{aligned}\langle \hat{a}_k \sigma_\mu^{(i)} \rangle &\simeq \langle \hat{a}_k \rangle \langle \sigma_\mu^{(i)} \rangle \\ \langle \hat{a}_k^\dagger \sigma_\mu^{(i)} \rangle &\simeq \langle \hat{a}_k^\dagger \rangle \langle \sigma_\mu^{(i)} \rangle\end{aligned}\quad (4)$$

with $\mu = \{x, y, z\}$. These approximations ignore the quantum correlations in the coupling between bosonic and spin modes.

Additionally defining the auxiliary variables $S_k(t) \equiv \sin(\omega_L t) \sum_j \Omega \eta_k^j \langle \sigma_x^{(j)} \rangle$ and $J^{(i)}(t) \equiv \sin(\omega_L t) \Omega (2 \sum_l \eta_l^i \langle \Re[\hat{a}_l] \rangle) + \varepsilon \delta_{p,i}$, we obtain the approximate equations of motion,

$$\begin{aligned}\frac{d\langle \Re[\hat{a}_k] \rangle}{dt} &= \omega_k \langle \Im[\hat{a}_k] \rangle, \\ \frac{d\langle \Im[\hat{a}_k] \rangle}{dt} &= -\omega_k \langle \Re[\hat{a}_k] \rangle - S_k(t), \\ \frac{d\langle \vec{\sigma}^{(i)} \rangle}{dt} &= -2 \begin{pmatrix} 0 & B(t) & 0 \\ -B(t) & 0 & J^{(i)}(t) \\ 0 & -J^{(i)}(t) & 0 \end{pmatrix} \cdot \langle \vec{\sigma}^{(i)} \rangle\end{aligned}\quad (5)$$

where a spin vector notation, $\langle \vec{\sigma}^{(i)} \rangle = (\langle \sigma_x^{(i)} \rangle, \langle \sigma_y^{(i)} \rangle, \langle \sigma_z^{(i)} \rangle)$, has been used. This is a system of $2 \times M + 3 \times N$ non-linear first-order ordinary differential equations. Hence, it is numerically solved with a first order, ordinary differential equation solver that uses the Gragg–Bulirsch–Stoer method, stepsize control and order selection, called ODEX [46].

B. Comparison of semiclassical approximation to full quantum evolution

To benchmark the semiclassical method, we have compared it against a full quantum evolution of the system using Krylov subspaces. The latter is a method to study the dynamical evolution under time-dependent Hamiltonians that computes a reduced evolution operator omitting contributions smaller than a certain threshold, that is, transitions to irrelevant states. Despite this neglect, the Krylov evolution can be considered an *exact* numerical simulation, as it iteratively determines which part of the Hilbert space is irrelevant at a given accuracy.

In both cases, semiclassical and full quantum, the evolution of a given initial state under a time-depending Hamiltonian is calculated with time steps in a recurrent way. In the fully quantum calculation, the time steps are of the order of 1 ns, while in the semiclassical description they are variable, but can be orders of magnitude larger. In the quantum case, we have to specify a quantum state—a complex vector in the joint Fock basis of phononic and spin modes—, containing the amplitudes of every state of the basis. In the semiclassical case, we only have to supply the initial mean values of every operator.

It should be noted that the exact quantum evolution requires truncating the maximum phonon number which

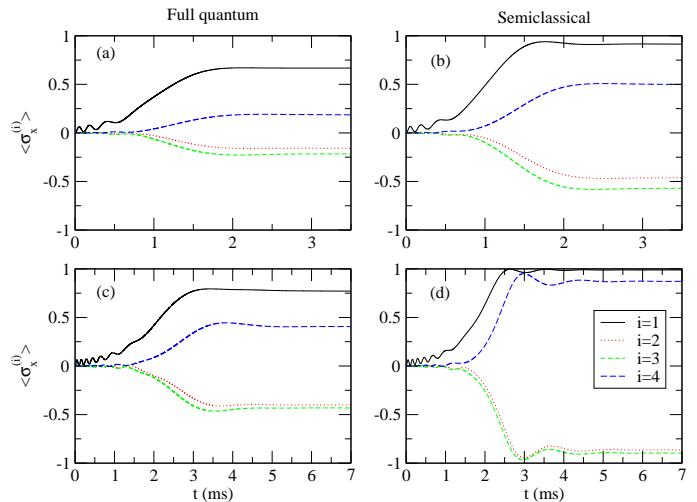


FIG. 2. Quantum (a,c) and semiclassical (b,d) evolution of $\langle \hat{\sigma}_x^{(i)} \rangle$. The figure is computed with $N = 4$ ions with a detuning $\delta = 2900$ kHz. Panels (a) and (b) correspond to $\tau = 0.35$ ms and panels (c) and (d) to $\tau = 0.7$ ms.

in our case was set to two phonons per mode. Such truncation of the Hilbert space requires sufficiently cool systems. And even with this truncation, the quantum evolution is restricted to a small number of ions. Considering only one transverse phonon branch, i.e. N phonon modes, with a maximum population of two phonons per mode, the Hilbert space dimension is $2^N \times 3^N$, that is, a dimension of 46656 for $N = 6$ ions. The semiclassical approach, in contrast, allows us to explore larger systems.

1. Time evolution of $\langle \hat{\sigma}_x^{(i)} \rangle$

The semiclassical model captures well the qualitative behavior of the evolution of $\langle \hat{\sigma}_x^{(i)} \rangle$, as exemplified in Fig. 2. In the figure we compare the semiclassical evolution with the exact dynamics for $N = 4$ ions for two different decay times. The discrepancy between semiclassical and exact evolution is smallest for shorter times ($t \lesssim \tau$), where the semiclassical model is able to correctly capture the details of the dynamical evolution, most notably little wiggles in the evolution of the biased ion, $i = 1$. Importantly, the semiclassical model also agrees with the exact evolution regarding general features such as the separation time, and the sign of each $\langle \hat{\sigma}_x^{(i)} \rangle$ in the long-time limit. As discussed in more detail in the next paragraph, this enables a quite accurate prediction of annealing fidelities, despite the fact that the approximation disregards some quantum properties. Thus it provides a computationally efficient way to study the behavior of larger systems.

For a better understanding of the errors in the semiclassical approach, we have exactly calculated the evolution of $\langle \hat{n}_3 \sigma_x^{(i)} \rangle$, see Fig. 3(a), and of $\langle \hat{n}_3 \rangle \langle \sigma_x^{(i)} \rangle$. As

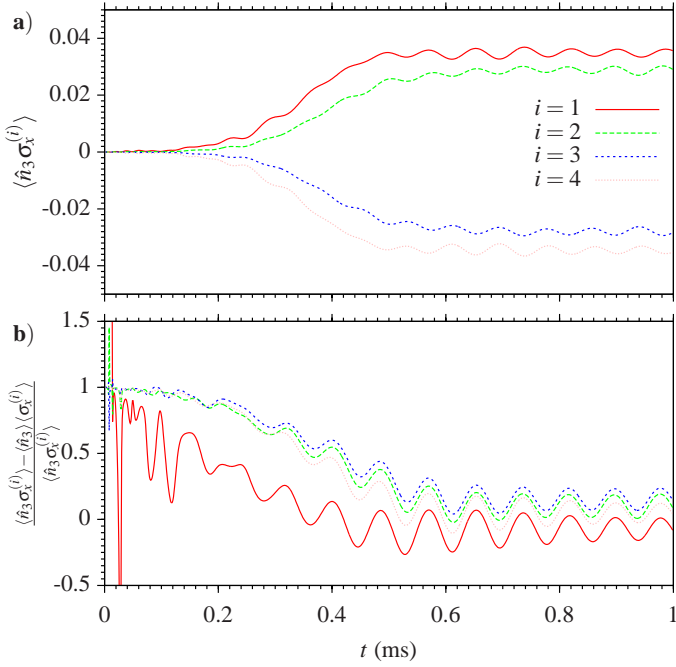


FIG. 3. Evolution of $\langle \hat{n}_3 \hat{\sigma}_x^{(i)} \rangle$ (a) and of the relative difference $(\langle \hat{n}_3 \hat{\sigma}_x^{(i)} \rangle - \langle \hat{n}_3 \rangle \langle \hat{\sigma}_x^{(i)} \rangle) / \langle \hat{n}_3 \hat{\sigma}_x^{(i)} \rangle$ for a system of four spins with initial populations of phonons set to zero for a detuning $\delta = 1000$ kHz.

our semiclassical approximation is based on substituting the former correlator by the latter one, the discrepancy between both expressions is an indicator for the quality of the semiclassical approach. In Fig. 3(b), we plot the relative difference as a function of time: Initially, the phonon and spin degrees of freedom are taken as uncorrelated, thus, the semiclassical and the exact description coincide at $t = 0$. On short time scales, both correlators have small absolute values, but their relative difference becomes large. For times larger than the separation time, the absolute values of the correlators increase, and the relative errors decrease. On long time scales, the errors oscillate around mean values of the order 0.1. This observation suggests that the main errors made in the semiclassical approximation are introduced at short times, where the transverse magnetic field and its temporal derivative takes large values.

2. Fidelity

As we have seen the semiclassical approximation provides a reasonable description of the dynamics in many configurations. Let us now explore in more detail in which parameter regions it predicts the correct fidelity for the annealing protocol. In Fig. 4 we present a comparison of the fidelities obtained from the exact time evolution and from the semiclassical approach for a system of four ions. We tune through a broad range of beatnote

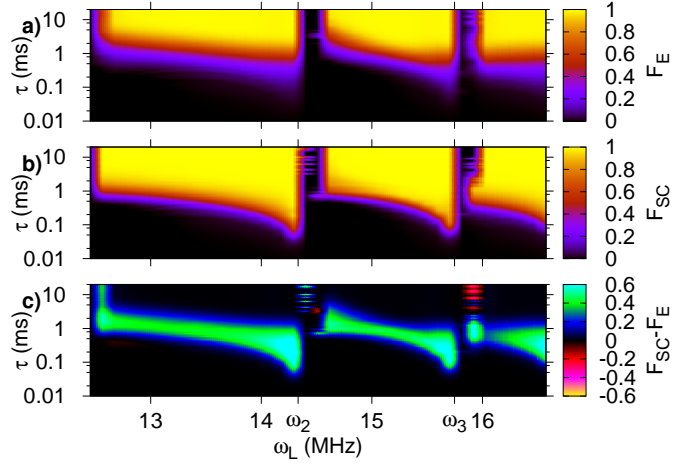


FIG. 4. Fidelity obtained with the full quantum evolution F_E (a), the semiclassical model F_{SC} (b), and the difference between the semiclassical model and the full quantum (c). In both cases, we consider a system of four ions, and we plot the magnitudes as a function of ω_L and τ . The fidelity is readout after a time 20τ .

frequencies ω_L , and vary the decay time τ of the magnetic field. The overall agreement is very good: Both methods predict a small fidelity when the field decays too fast (small τ), or when the system is too close to one of the phonon resonances. The semiclassical evolution, however, slightly overestimates the fidelity for small τ , and also slightly below each phonon resonance, that is, on the ferromagnetic side of the resonance. Notably, the semiclassical approach works quite well in the glassy regimes above the resonances, where it estimates correctly the regions in which the annealer fails for any annealing time.

As discussed earlier, the failure of the annealing protocol for small τ is due to non-adiabatic behavior in the fast varying field. The failure near the resonance, though, cannot be fixed by increasing τ , and has its origin in the deviation from of the Dicke dynamics from the effective spin model. Although such deviations are expected on both sides of a phonon resonance, the region of zero fidelity is seen only on the glassy side of each resonance. From that perspective, the size of the spin gap seems to play a role as well, although in this regime we should not compare it to \hbar/τ , but to those spin-phonon energy scales which are neglected in the effective spin model, that is, the first order term in a Magnus expansion, see Ref. [47].

The main advantage of the semiclassical model is that it can easily be applied to larger systems. In Fig. 5, we consider systems of six and eight ions. Notably, a broad region of zero fidelity occurs for eight ions between ω_5 and ω_6 . Its origin is unclear to us, and further calculations on the fully quantum evolution would be needed in order to discriminate whether they are true effects or merely calculation artifacts.

We finish this section by discussing the factor which limits the scalability of the quantum annealer. As seen

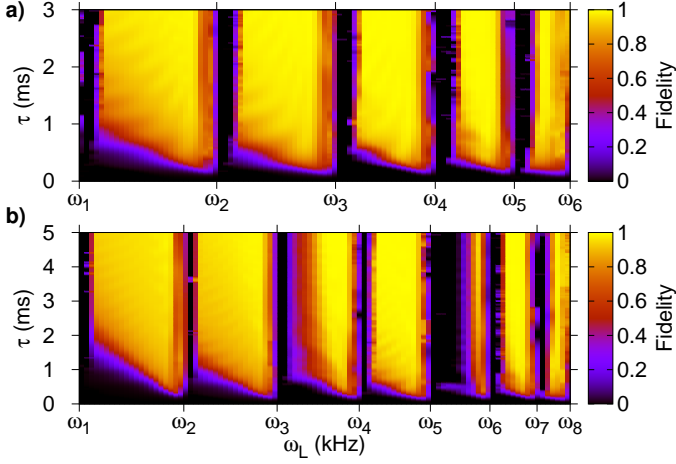


FIG. 5. Fidelity of a system of six ions (a) and a system of eight ions (b) as a function of ω_L and τ using the semiclassical approximation. Final times are 20τ .

above, below a critical detuning from the resonance the fidelity drops to zero. This sets a limit to the scalability of the quantum annealer, because, with the number of modes being proportional to the number of ions, the mode spacing decreases when the system size is increased. However, we note that phonon spectra are not equidistant, and within the transverse branch, the phonon spacing is largest at the lower energetic end of the phonon spectrum. Thus, to achieve finite fidelity in an up-scaled system, one may need to operate in the regime of low-energy phonons. The semiclassical estimates in Ref. [40] suggest that the quantum annealing still works in systems with more than twenty ions, presumably large enough to detect quantum speed-up.

IV. FINITE TEMPERATURE EFFECTS ON THE ANNEALING PROTOCOL

Finite temperature effects are expected to reduce the quality of the annealing protocol, recently, however, thermal effects are shown to aid the annealing protocol for a 16-qubit problem in a superconducting setup [48]. In this section we study the robustness of the annealing protocol when the phonons are initially at finite temperature. To do so, we consider an initial state with phonon mode populations set as follows: we fix the temperature T of the phonons, then, the mean values of the number of phonons for each mode are sampled according to the a bosonic thermal bath probability distribution at T . With these initial conditions, the system is then evolved semiclassically according to Eqs. (5). This process is repeated with different initial values of the population of phonons, sampled appropriately. After the evolution, the statistical moments are calculated in order to infer the thermal properties of the system at the final time.

It should be noted that our dynamical model only cap-

tures the coherent Hamiltonian evolution, but no decoherence processes due to interactions with the environment. Thus, in order to account for all thermal effects, heating events, as they occur for instance due to trap inhomogeneties, should be taken into account by considering an increased initial temperature.

A. Classical thermal phonons

We assume that the initial populations of the phononic modes are determined by a phonon temperature. In the canonical ensemble, the expected value of the number operator of the phonons in the k -th mode is,

$$\langle \hat{n}_k \rangle = \frac{1}{e^{\beta \hbar \omega_k} - 1}. \quad (6)$$

The corresponding Hamiltonian of the symmetrized phonon field is $\hat{H}_{\text{ph}} = \hbar \sum_k \omega_k \frac{\hat{a}_k^\dagger \hat{a}_k + \hat{a}_k \hat{a}_k^\dagger}{2}$. The expected value of the annihilation operator $\alpha_k \equiv \langle \hat{a}_k \rangle$ is sampled as,

$$P(\alpha_k) = \frac{1}{\pi \langle \hat{n}_k \rangle} e^{-\frac{|\alpha_k|^2}{\langle \hat{n}_k \rangle}}. \quad (7)$$

The complex-valued Gaussian probability distribution function (PDF) for the random variable α_k is a product of two Normal PDFs—one real the other purely imaginary—for the random variables $\Re[\alpha_k]$ and $\Im[\alpha_k]$. Both distributions have a mean $\mu = 0$ and variance $\sigma^2 = \hat{n}_k/2$. We thus use for convenience,

$$P(\alpha_k) = N(\Re[\alpha_k]; 0, \langle \hat{n}_k \rangle / 2) N(\Im[\alpha_k]; 0, \langle \hat{n}_k \rangle / 2), \quad (8)$$

being $N(x; \mu, \sigma^2)$ the Normal PDF of the random variable x with mean μ and variance σ^2 .

B. Effects of temperature on the protocol

To evaluate the effects of temperature on the proposed annealing protocol we will consider different initial temperatures and detunings. In all cases we will fix the decay time $\tau = 10$ ms. Fig. 6 shows the fidelity and the total phononic population per mode in the system. In the figure we compare results obtained with several values of ω_L and a broad range of temperatures of the phonons. Quite generally, panels (a) and (b) show that up to a certain temperature the fidelity is not affected by thermal phonons, but above this temperature the fidelity drops to zero. The value of this temperature strongly depends on the detuning, and decreases by several orders of magnitudes when we change from a far-detuned configuration to a near-resonance scenario. For instance, in the far-detuned regime at $\omega_L = \omega_2 - 902.41$ kHz (solid squares) the critical temperature is of the order 0.1 K, while close to the resonance at $\omega_L = \omega_2 - 35.33$ kHz (small triangles), the fidelity drop occurs at a temperature of the

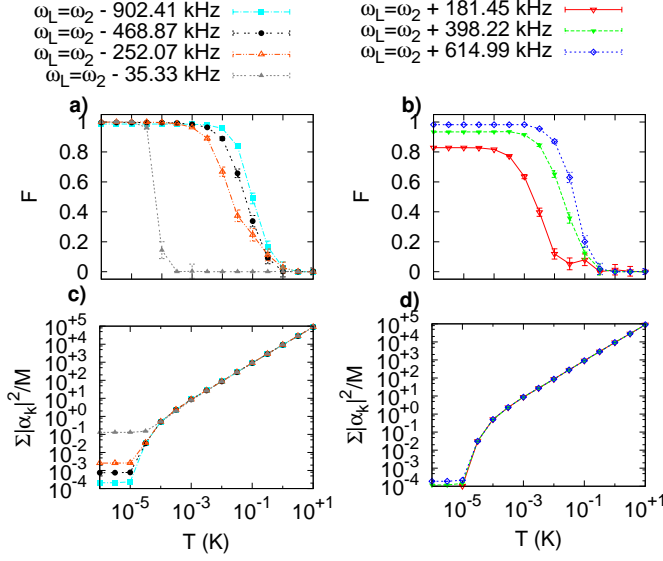


FIG. 6. We plot the fidelity (a,b) and the square of the phonon coherences (c,d), as a function of the initial phonon temperature, as obtained from the semiclassical calculation for a system of four ions. Different lines correspond to different detunings. Panels (a) and (c) consider cases where the second phonon resonance is approached from below (where the magnetic order is ferromagnetic), while panels (b) and (d) consider cases where the same resonance is approached from above (where a glassy regime occurs near the resonance). In our system, the second resonance occurs at a frequency $\omega_2 = 14332.7$ kHz. All calculations were done for $\tau = 10$ ms. Each point is obtained by sampling over 1,000 runs. The adscribed error is 2σ .

order 10^{-4} K. Such behavior is seen both when we approach the phonon resonance from above (panel (b)) or below (panel (a)), but we remind that above the resonance there is a finite region in which the fidelity is zero even at $T = 0$, cf. the discussion of Fig.(4) in Sec. II B 2.

Regarding the phonon population, we assume that a reasonable estimate of $\langle \hat{n}_k \rangle$ is given by $|\alpha_k|^2$, as would be the case if the phonon field remains coherent. In Fig. 6(c,d), we may distinguish two different regimes: At low temperatures, i.e. for $T \lesssim 10^{-5}$ K, the final phonon population is dominated by those phonons which are produced by the spin-phonon coupling. The number of those phonons is independent from the temperature, and as shown earlier in Fig. 1(b), such phonons are generated also at $T = 0$. The proximity to the resonance induces a larger population of the dominant mode, resulting in a larger value for the population as we approach the resonance. In contrast, for high temperatures, the phonon population is dominated by thermal phonons present already in the beginning of the evolution. In this case, the phonon population is more or less constant during the evolution, and the population number strongly depends on the temperature, according to the

initial values from the Boltzmann distribution. As in this case, the time evolution does not noticeably change the phonon distribution, initial and final distribution are very close, and so are initial and final temperature. Between the low- and high- temperature phase, there is a narrow crossover regime, where the number of dynamically generated phonons is similar to the number of thermal phonons. The temperature at which this happens generally depends on the detuning, i.e. on ω_L . In all cases, the fidelity drop occurs only in the high-temperature regime, that is, the number of thermal photons must be large compared to the dynamically generated phonons in order to negatively affect the spin evolution.

C. Thermal tolerance of the Lamb-Dicke regime

The Hamiltonian Eq. (1) describes the trapped ion system when it is in the Lamb-Dicke regime, that is, for $kx \ll 1$. In a harmonic oscillator with frequency ω , we have $\langle x^2 \rangle = \frac{\hbar}{m\omega} (\langle n \rangle + \frac{1}{2})$. With $k = \sqrt{2m\omega_{\text{rec}}/\hbar}$, and introducing the Lamb-Dicke parameter $\eta = \sqrt{\omega_{\text{rec}}/\omega}$, we re-write the Lamb-Dicke condition as

$$\eta \sqrt{2\langle n \rangle + 1} \ll 1. \quad (9)$$

All phonon frequencies ω are of the order of the radial trap frequency, $\omega_{\text{rad}} = 2\pi \times 2,655$ kHz. In our simulation, the recoil frequency is taken as $\omega_{\text{rec}} = 2\pi \times 15$ kHz, so we obtain a Lamb-Dicke parameter $\eta \approx 0.075$. Thus, the Lamb-Dicke regime requires $\sqrt{\langle n \rangle + 0.5} \ll 10$, which is fulfilled by a phonon occupation $\langle n \rangle \lesssim 1$. From that perspective, we have to disregard those calculations where the phonon population exceeds this number. From Fig. 6(c,d) we find that, for the Rabi frequency we have used, phonon numbers above 1 occur in the thermally dominated regime, independent from the detuning. This regime is characterized by temperatures $> 10^{-4}$ K.

V. SUMMARY AND CONCLUSIONS

We have considered a chain of trapped ions with an internal state (“spin”) coupled to vibrational modes via Raman lasers. The couplings are such that the effective model describing the ions is a long range spin model with tunable, pseudo-random couplings, leading to a spin-glass-like phase. The goal of our approach is the adiabatic distillation of the ground state in the glassy phase starting from a completely paramagnetic state. To this aim we consider the addition of a time-dependent transverse magnetic field. Our procedure goes as follows: At the initial time, the magnetic field is strong enough to ensure the ground state of the spins is a ferromagnetic state, with all spins aligned in the transverse direction. As time evolves we slowly, ideally adiabatically, remove the magnetic field such that the final Hamiltonian is our effective long-range spin model in the spin-glass-like phase.

We have simulated our annealing protocol using the exact evolution by means of a Krylov subspace method which is feasible for a small number of ions. In order to consider larger systems as well as to study the effect of temperature on the time evolution we have developed a semiclassical formalism which ignores the quantum correlations between the ions and the phonons. The quality of this method has been benchmarked by comparing its predictions with the exact evolution for four ions. The semiclassical model is found to provide a very accurate qualitative picture of our proposed method, and allows us to correctly identify the parameter region where the annealing protocol works well. By means of the semiclassical model we have thus extended our study to larger number of ions, providing an accurate picture of the ability of the annealing protocol to find the correct ground state depending on the annealing time.

Finally, the semiclassical model has allowed us to study the robustness of the scheme for initial phonon states at finite temperature. We find that the effect of temperature strongly depends on the detuning from a phonon resonance. While in most configurations, the quantum annealing does not break down within the Lamb-Dicke regime, close to a resonance the situation is different. Here, the fidelity of the annealing may drop even be-

fore the Lamb-Dicke limit is reached, see Fig. 6. Thus, while state-of-art spin model simulations which are carried out far off any phonon resonance (e.g. Refs. [22, 25]) require only cooling to the Lamb-Dicke limit, quantum annealing in the interesting glassy regime requires more cooling. Accordingly, our finding motivates the development of new, more efficient cooling techniques, as for instance cooling based on electromagnetically-induced transparency [49–51], which is very well suited to simultaneously achieve low populations in all radial modes.

ACKNOWLEDGMENTS

This work has been funded by EU grants (EQuaM (FP7-ICT-2013-C No. 323714), OSYRIS (ERC-2013-AdG No. 339106), SIQS (FP7-ICT-2011-9 No. 600645), and QUIC (H2020-FETPROACT-2014 No. 641122)), Spanish Ministerio de Economía y Competitividad grants (Severo Ochoa (SEV-2015-0522), FOQUS (FIS2013-46768-P), FIS2014-54672-P and FISICATEAMO (FIS2016-79508-P)), Generalitat de Catalunya (2014 SGR 401, 2014 SGR 874, and CERCA program), and Fundació Cellex. TG acknowledges support of the NSF through the PFC@JQI.

-
- [1] A. Acín, I. Bloch, H. Buhrman, T. Calarco, C. Eichler, J. Eisert, D. Esteve, N. Gisin, S. J. Glaser, F. Jelezko, S. Kuhr, M. Lewenstein, M. F. Riedel, P. O. Schmidt, R. Thew, A. Wallraff, I. Walmsley, and F. K. Wilhelm, ArXiv e-prints (2017), arXiv:1712.03773 [quant-ph].
 - [2] R. Barends, J. Kelly, A. Megrant, A. Veitia, D. Sank, E. Jeffrey, T. C. White, J. Mutus, A. G. Fowler, B. Campbell, Y. Chen, Z. Chen, B. Chiaro, A. Dunsworth, C. Neill, P. O'Malley, P. Roushan, A. Vainsencher, J. Wenner, A. N. Korotkov, A. N. Cleland, and J. M. Martinis, *Nature* **508**, 500 EP (2014).
 - [3] N. M. Linke, D. Maslov, M. Roetteler, S. Debnath, C. Figgatt, K. A. Landsman, K. Wright, and C. Monroe, *Proceedings of the National Academy of Sciences* **114**, 3305 (2017).
 - [4] C. Monroe and J. Kim, *Science* **339**, 1164 (2013).
 - [5] M. H. Devoret and R. J. Schoelkopf, *Science* **339**, 1169 (2013).
 - [6] S. Kirkpatrick, C. D. Gelatt, and M. P. Vecchi, *Science* **220**, 671 (1983).
 - [7] V. Černý, *Journal of Optimization Theory and Applications* **45**, 411 (1985).
 - [8] J. Brooke, D. Bitko, T. F. Rosenbaum, and G. Aeppli, *Science* **284**, 779 (1999), <http://science.sciencemag.org/content/284/5415/779.full.pdf>.
 - [9] T. Kadowaki and H. Nishimori, *Phys. Rev. E* **58**, 5355 (1998).
 - [10] E. Farhi, J. Goldstone, S. Gutmann, J. Lapan, A. Lundgren, and D. Preda, *Science* **292**, 472 (2001), <http://science.sciencemag.org/content/292/5516/472.full.pdf>.
 - [11] T. Albash and D. A. Lidar, *Rev. Mod. Phys.* **90**, 015002 (2018).
 - [12] M. W. Johnson, M. H. S. Amin, S. Gildert, T. Lanting, F. Hamze, N. Dickson, R. Harris, A. J. Berkley, J. Johansson, P. Bunyk, E. M. Chapple, C. Enderud, J. P. Hilton, K. Karimi, E. Ladizinsky, N. Ladizinsky, T. Oh, I. Perminov, C. Rich, M. C. Thom, E. Tolkacheva, C. J. S. Truncik, S. Uchaikin, J. Wang, B. Wilson, and G. Rose, *Nature* **473**, 194 (2011).
 - [13] T. F. Rønnow, Z. Wang, J. Job, S. Boixo, S. V. Isakov, D. Wecker, J. M. Martinis, D. A. Lidar, and M. Troyer, *Science* **345**, 420 (2014).
 - [14] S. Boixo, T. F. Rønnow, S. V. Isakov, Z. Wang, D. Wecker, D. A. Lidar, J. M. Martinis, and M. Troyer, *Nature Physics* **10**, 218 EP (2014), article.
 - [15] T. M. Lanting, “D-wave 2000q,” *Adiabatic Quantum Computing Conference 2017 (AQC 2017)*.
 - [16] T. M. Lanting, S. Boixo, S. V. Isakov, Z. Wang, D. Wecker, D. A. Lidar, J. M. Martinis, and M. Troyer, *Phys. Rev. Lett.* **87**, 257904 (2001).
 - [17] D. Porras and J. I. Cirac, *Phys. Rev. Lett.* **92**, 207901 (2004).
 - [18] A. Friedenauer, H. Schmitz, J. T. Glueckert, D. Porras, and T. Schaetz, *Nat. Phys.* **4**, 757 (2008).
 - [19] M. Mielenz, H. Kalis, M. Wittmer, F. Hakelberg, U. Warring, R. Schmied, M. Blain, P. Maunz, D. L. Moehring, D. Leibfried, and T. Schaetz, *Nat. Commun.* **7**, ncomms11839 (2016).
 - [20] H. Kalis, F. Hakelberg, M. Wittmer, M. Mielenz, U. Warring, and T. Schaetz, *Phys. Rev. A* **94**, 023401 (2016).
 - [21] A. Lambrecht, J. Schmidt, P. Weckesser, M. Debatin, L. Karpa, and T. Schaetz, *Nature Photonics* **11**, 704 (2017).
 - [22] P. Jurcevic, H. Shen, P. Hauke, C. Maier, T. Brydges, C. Hempel, B. P. Lanyon, M. Heyl, R. Blatt, and C. F. Roos, *Phys. Rev. Lett.* **119**, 080501 (2017).

- [23] H.-K. Li, E. Urban, C. Noel, A. Chuang, Y. Xia, A. Ransford, B. Hemmerling, Y. Wang, T. Li, H. Häffner, and X. Zhang, *Phys. Rev. Lett.* **118**, 053001 (2017).
- [24] J. Zhang, P. W. Hess, A. Kyprianidis, P. Becker, A. Lee, J. Smith, G. Pagano, I.-D. Potirniche, A. C. Potter, A. Vishwanath, N. Y. Yao, and C. Monroe, *Nature* **543**, 217 (2017).
- [25] J. Zhang, G. Pagano, P. W. Hess, A. Kyprianidis, P. Becker, H. Kaplan, A. V. Gorshkov, Z.-X. Gong, and C. Monroe, *Nature* **551**, 601 EP (2017).
- [26] A. Safavi-Naini, R. J. Lewis-Swan, J. G. Bohnet, M. Gärttner, K. A. Gilmore, E. Jordan, J. Cohn, J. K. Freericks, A. M. Rey, and J. J. Bollinger, *ArXiv e-prints* (2017), arXiv:1711.07392 [quant-ph].
- [27] D. Walls and G. Milburn, *Quantum Optics*, 2nd ed. (Springer, 2008).
- [28] A. Piñeiro Orioli, A. Safavi-Naini, M. L. Wall, and A. M. Rey, *Phys. Rev. A* **96**, 033607 (2017).
- [29] M. L. Wall, A. Safavi-Naini, and A. M. Rey, *Phys. Rev. A* **95**, 013602 (2017).
- [30] M. Gärttner, J. G. Bohnet, A. Safavi-Naini, M. L. Wall, J. J. Bollinger, and A. M. Rey, *Nature Physics* **13**, 781 EP (2017), article.
- [31] M. L. Wall, A. Safavi-Naini, and A. M. Rey, *Phys. Rev. A* **94**, 053637 (2016).
- [32] T. Graß, A. Celi, G. Pagano, and M. Lewenstein, *Phys. Rev. A* **97**, 010302 (2018).
- [33] T. Graß, M. Lewenstein, and A. Bermudez, *New Journal of Physics* **18**, 033011 (2016).
- [34] T. Graß, C. Muschik, A. Celi, R. W. Chhajlany, and M. Lewenstein, *Phys. Rev. A* **91**, 063612 (2015).
- [35] P. Nevado, S. Fernández-Lorenzo, and D. Porras, *Phys. Rev. Lett.* **119**, 210401 (2017).
- [36] P. Nevado and D. Porras, *Phys. Rev. A* **92**, 013624 (2015), arXiv:1503.04614 [quant-ph].
- [37] P. Nevado and D. Porras, *Phys. Rev. A* **93**, 013625 (2016).
- [38] A. Lemmer, C. Cormick, D. Tamascelli, T. Schaetz, S. F. Huelga, and M. B. Plenio, *ArXiv e-prints* (2017), arXiv:1704.00629 [quant-ph].
- [39] P. Hauke, L. W. Bonnes, M. Heyl, and W. Lechner, *Frontiers in Physics* **3**, 21 (2015).
- [40] T. Graß, D. Raventós, B. Juliá-Díaz, C. Gogolin, and M. Lewenstein, *Nat. Comms.* **7** (2016), 10.1038/ncomms11524.
- [41] F. Barahona, *Journal of Physics A: Mathematical and General* **15**, 3241 (1982).
- [42] L. C. Venuti, T. Albash, D. A. Lidar, and P. Zanardi, *Phys. Rev. A* **93**, 032118 (2016).
- [43] K. Nishimura, H. Nishimori, A. J. Ochoa, and H. G. Katzgraber, *Phys. Rev. E* **94**, 032105 (2016).
- [44] K. Nishimura and H. Nishimori, *Phys. Rev. A* **96**, 042310 (2017).
- [45] N. Chancellor, S. Szoke, W. Vinci, G. Aeppli, and P. A. Warburton, *Scientific Reports* **6**, 22318 (2016).
- [46] E. Hairer, S. P. Nørsett, and G. Wanner, *Solving Ordinary Differential Equations I. Nonstiff Problems.*, 2nd ed., Springer Series in Comput. Mathematics (Springer-Verlag, Berlin Heidelberg, 1993).
- [47] K. Kim, M.-S. Chang, R. Islam, S. Korenblit, L.-M. Duan, and C. Monroe, *Phys. Rev. Lett.* **103**, 120502 (2009).
- [48] N. G. Dickson, M. W. Johnson, M. H. Amin, R. Harris, F. Altomare, A. J. Berkley, P. Bunyk, J. Cai, E. M.

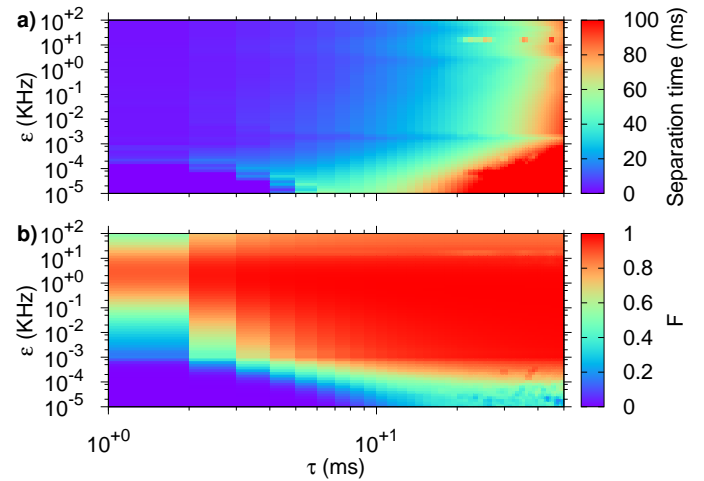


FIG. 7. Separation time (a)) and Fidelity (b)) of systems with 6 spins for several values of ϵ and τ , with initial populations of phononic modes set to 0. Waiting time is fixed to 20τ and $\omega_L = \omega_N - 1500$ kHz.

- Chapple, P. Chavez, F. Cioata, T. Cirip, P. deBuen, M. Drew-Brook, C. Enderud, S. Gildert, F. Hamze, J. P. Hilton, E. Hoskinson, K. Karimi, E. Ladizinsky, N. Ladizinsky, T. Lanting, T. Mahon, R. Neufeld, T. Oh, I. Perminov, C. Petroff, A. Przybysz, C. Rich, P. Spear, A. Tcaciuc, M. C. Thom, E. Tolkacheva, S. Uchaikin, J. Wang, A. B. Wilson, Z. Merali, and G. Rose, *Nature Communications* **4**, 1903 (2013).
- [49] C. F. Roos, D. Leibfried, A. Mundt, F. Schmidt-Kaler, J. Eschner, and R. Blatt, *Phys. Rev. Lett.* **85**, 5547 (2000).
- [50] Y. Lin, J. P. Gaebler, T. R. Tan, R. Bowler, J. D. Jost, D. Leibfried, and D. J. Wineland, *Phys. Rev. Lett.* **110**, 153002 (2013).
- [51] R. Lechner, C. Maier, C. Hempel, P. Jurcevic, B. P. Lanyon, T. Monz, M. Brownnutt, R. Blatt, and C. F. Roos, *Phys. Rev. A* **93**, 053401 (2016).

Appendix A: Robustness of the semiclassical calculation

One can test the quality of the integration method by checking whether the constants of motion are conserved. In time-independent systems, the total energy of the system is usually the conserved quantity which can be computed most easily. Unfortunately, since the Hamiltonian in Eq. 1 does not commute with itself at different times due to the transverse magnetic field in the annealing term, the total energy of the system is not conserved. Furthermore, it is challenging to find an analytical expression for an alternative conserved quantity given the infinitely non-commutativity of the Pauli matrices algebra. We have tested the integration method checking its time reversibility. The latter test has given relative differences below 10^{-7} , which is within the range of the computation

precision.

Appendix B: Optimal bias for the exponential annealing function

Although the only function of the bias potential ϵ is to break Z_2 symmetry in the target Hamiltonian, it turns out that the value and position of the bias have a non-negligible effect on the outcome of the annealing process. Here, we investigate which values of the bias ϵ and the annealing parameter τ minimize the separation time. As seen in Fig. 7 a), the separation time is minimized for

smaller values of τ , at any value of the bias larger than Hz. However, small τ are known to affect negatively the fidelity. As we see from Fig. 7 b), there is, even for decay times as short as a few ms, a range of bias potentials (roughly between 1 kHz and 10 kHz), where the fidelity gets large. Thus, this range defines the optimal choice for ϵ , which we have also used in our calculations.

We also note that the magnitude of the bias provides a bound for the maximum absolute value of $\langle\sigma_x\rangle$, that is, the spin expectation on the biased site at the end of the annealing depends on the strength of the bias potential. For a weak bias, this spin will deviate only weakly from zero, limiting the overall fidelity.